ARTICLES
PUBLISHED ONLINE: 15 FEBRUARY 2016 | DOI: 10.1038/NPHOTON.2015.281
nature photonics

A fully reconfigurable photonic integrated signal processor

Weilin Liu[1‡], Ming Li[1†‡], Robert S. Guzzon[2‡], Erik J. Norberg[2], John S. Parker[2], Mingzhi Lu[2], Larry A. Coldren[2] and Jianping Yao[1*]

Photonic signal processing has been considered a solution to overcome the inherent electronic speed limitations. Over the past few years, an impressive range of photonic integrated signal processors have been proposed, but they usually offer limited reconfigurability, a feature highly needed for the implementation of large-scale general-purpose photonic signal processors. Here, we report and experimentally demonstrate a fully reconfigurable photonic integrated signal processor based on an InP–InGaAsP material system. The proposed photonic signal processor is capable of performing reconfigurable signal processing functions including temporal integration, temporal differentiation and Hilbert transformation. The reconfigurability is achieved by controlling the injection currents to the active components of the signal processor. Our demonstration suggests great potential for chip-scale fully programmable all-optical signal processing.

One of the fundamental challenges for digital signal processing (DSP) is the limited speed, largely restricted by the electronic sampling rate. In an optical network, signal processing is implemented based on DSP, which involves electronic sampling, optical-to-electrical (OE) and electrical-to-optical (EO) conversions. A solution to achieve power-efficient and high-speed signal processing in an optical network is to implement signal processing directly in the optical domain using a photonic signal processor to avoid the need for electronic sampling, OE and EO conversions[1–3]. Numerous photonic signal processors have so far been reported based on either discrete components or photonic integrated circuits[1–10]. Photonic signal processors based on discrete components usually have decent programming abilities but are more bulky and less power efficient, whereas a photonic integrated signal processor has a much smaller footprint and a higher power efficiency. A photonic signal processor can be used to implement fundamental signal generation and processing functions such as optical pulse shaping and arbitrary waveform generation[1], optical dispersion compensation[7], temporal integration[8], temporal differentiation[9] and Hilbert transformation[10]. These functions are basic building blocks of a general-purpose signal processor for signal generation and fast computing. Fast computing processes such as temporal integration, temporal differentiation and Hilbert transformation have important applications[11–22]. For example, a photonic integrator is a device that is able to perform the time integral of an optical signal, which has applications in dark soliton generation[12], optical memory[13] and optical analog–digital conversion[14]. One of the most important characteristic parameters of a photonic integrator is the integration time. A long integration time means a better integration capability. An ideal photonic temporal integrator should have an infinite integration time. An on-chip all-optical integrator compatible with complementary metal oxide–semiconductor (CMOS) technology was reported[15], based on an add-drop ring resonator with an integration time of 800 ps. For many applications, however, an integration time as long as a few nanoseconds is needed. To achieve such a long integration time, the insertion loss must be precisely compensated to obtain a high Q-factor, which is very challenging, particularly for stable operation without causing lasing. In addition, an integrator with a fractional or higher order is also needed, which is more difficult to implement[16]. A photonic temporal differentiator[17] is a device that performs temporal differentiation of an optical signal, and has applications in all-optical Fourier transform[18,19], temporal pulse characterization[20] and the demultiplexing of an optical time division multiplexed (OTDM) signal[21], for example. A photonic Hilbert transformer is a device that derives the analytic representation of a signal[10], and has been widely used for single-sideband (SSB) modulation. Optical SSB modulation is particularly useful in a radio-over-fibre (ROF) link to avoid dispersion-induced power fading[22]. Although the photonic implementations of these functions have been reported[8–10,15,17], a signal processor is usually designed to perform a specific function with no or very limited reconfigurability. For general-purpose signal processing, however, a photonic signal processor should be able to perform multiple functions with high reconfigurability.

In this Article, we report the design, fabrication and experimental demonstration of a fully reconfigurable photonic integrated signal processor to perform the three signal processing functions introduced above. The photonic signal processor consists of three active microring resonators (R1, R2, and R3) and a bypass waveguide as a processing unit cell, as shown in Fig. 1a,b. To obtain on-chip reconfigurability, we incorporate nine semiconductor optical amplifiers (SOAs) and twelve current-injection phase modulators (PMs) in the unit cell, as shown in Fig. 1b. The tunable coupling between two neighbouring rings and between the outer ring and the bypass waveguide is realized using four tunable couplers (TCs) with each consisting of two multi-mode interference (MMI) couplers and two PMs, as shown in the inset in Fig. 1b. The coupling ratio in each TC can be tuned by adjusting the injection currents to the two PMs in the TC. Within each ring there are two SOAs used to compensate for the waveguide propagation loss and the MMI splitting loss and insertion loss. When an SOA is forward biased it can create an optical gain. On the

[1]Microwave Photonics Research Laboratory, University of Ottawa, Ottawa, Ontario K1N 6N5, Canada. [2]Department of Electrical and Computer Engineering, University of California Santa Barbara, Santa Barbara, California 93116, USA. [†]Present address: State Key Laboratory on Integrated Optoelectronics, Institute of Semiconductors, Chinese Academy of Sciences, Beijing 100083, China. [‡]These authors contributed equally to this work.
*e-mail: jpyao@eecs.uottawa.ca

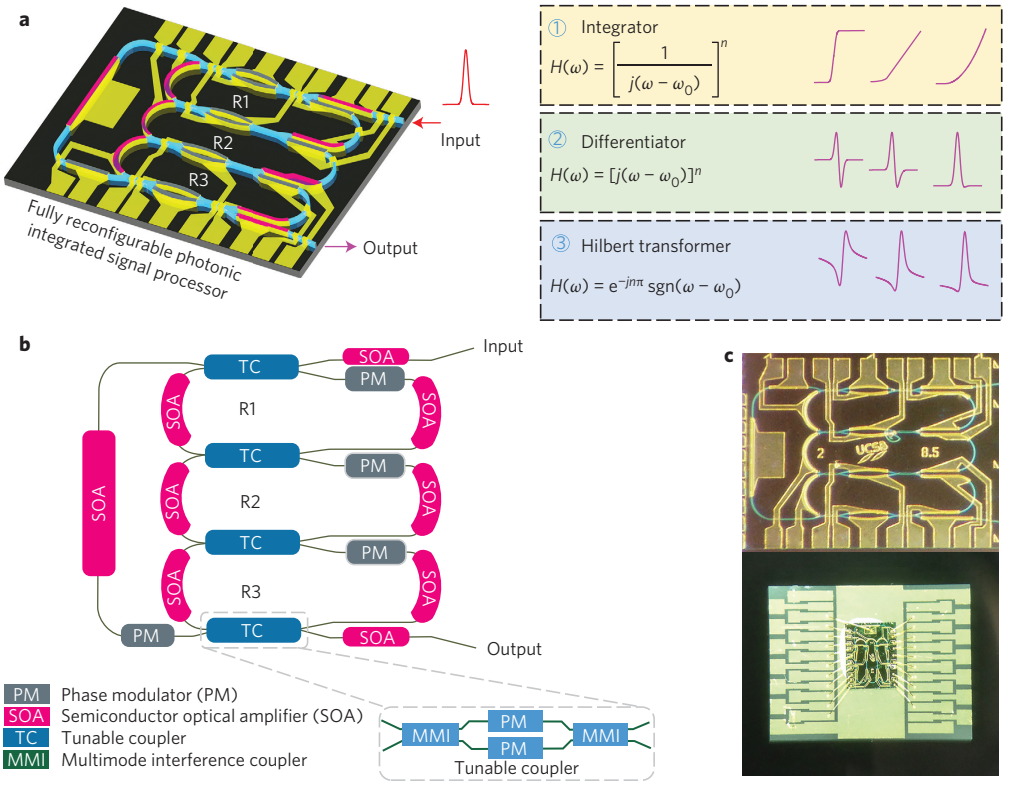

Figure 1 | The schematics of the proposed photonic integrated signal processor. a, The schematic diagram of the processor as a unit cell. **b**, A schematic representation of the processor consisting of three coupled rings and a bypass waveguide. **c**, The fabricated on-chip photonic signal processor prototype. The lower image shows the chip wire bonded to a carrier for experimental test.

other hand, an SOA can operate as an optical absorber when it is reverse biased, which is the key to achieving the configurability of the processor. Consequently, with the SOAs used in this design, a waveguide path could be on or off to facilitate the synthesis of various circuit geometries. By reverse biasing one SOA in each of the three ring resonators, for example, the three mutually coupled rings are reduced to a single optical path. With the bypass waveguide incorporated in the design, the chip can be reconfigured as a Mach–Zehnder interferometer (MZI). The signal processing functions can be implemented by reconfiguring the unit cell with a specific geometry (see Supplementary Section 1). In addition, there is a current-injection PM in each ring resonator, and a PM in the bypass waveguide, which are used to achieve wavelength tunability. Furthermore, the order of the signal processor, either a fractional or higher order, can be tuned by tuning the coupling ratio of the TC. The fabricated device, shown in Fig. 1c, is wire-bonded to a carrier to enable easy access to the SOAs and PMs with the assistance of a customized probe station. In the following, the proposed integrated photonic signal processor reconfigured to achieve three different functions for fast signal processing is discussed.

Photonic temporal integrator

An nth-order temporal integrator is a linear time-invariant (LTI) system with a transfer function given by[16]

$$H_n(\omega) = \left[\frac{1}{j(\omega - \omega_0)}\right]^n \quad (1)$$

where $j = \sqrt{-1}$, ω is the optical angular frequency and ω_0 is the carrier frequency of the signal to be processed. A first-order photonic temporal integrator can be implemented using an optical resonator, for example, an add-drop ring resonator[16] (see Supplementary Section 3-I). If the input and drop ports are used, the ring resonator would have a spectral response that is close to that given in (equation (1)) for $n = 1$, and it is a first-order temporal integrator. A higher-order (with $n = 2, 3, \ldots$) temporal integrator can be implemented by cascading or coupling n first-order integrators[16]. An nth-order temporal integrator is capable of calculating the nth time integral of an arbitrary optical waveform.

The photonic integrated signal processor shown in Fig. 1 can be configured to operate as a temporal integrator with an order of 1, 2 or 3, depending on the number of rings used. In the unit cell, there are three mutually coupled ring resonators with two active SOAs in each ring resonator. If one SOA in a ring resonator is reverse-biased to shut off the waveguide, the ring resonator simply becomes a waveguide. By controlling the number of rings in the unit cell to be 1, 2 or 3, a temporal integrator with an order of 1, 2 or 3 is achieved (see Supplementary Sections 3-II, III). For example, a temporal integrator with an order of 1 is configured by shutting off two ring resonators, as shown in Fig. 2a. In each ring resonator, a current injection PM is incorporated that is used to tune the resonance frequency of the ring resonator, thus achieving wavelength tunability. In addition, the tunable coupling between two adjacent rings, and between an outer ring (R1 or R3) and the bypass waveguide, can offer tunable spectral response of the coupled-ring resonator, which can be used to achieve higher-order integrators.

Photonic temporal differentiator

An nth-order temporal differentiator provides the nth-order time derivative of the envelope of an optical signal. An nth-order temporal differentiator can be considered as an LTI system with a transfer function given by

$$H_n(\omega) = [j(\omega - \omega_0)]^n = \begin{cases} e^{jn(\pi/2)}|\omega - \omega_0|^n & \omega > \omega_0 \\ e^{-jn(\pi/2)}|\omega - \omega_0|^n & \omega < \omega_0 \end{cases} \quad (2)$$

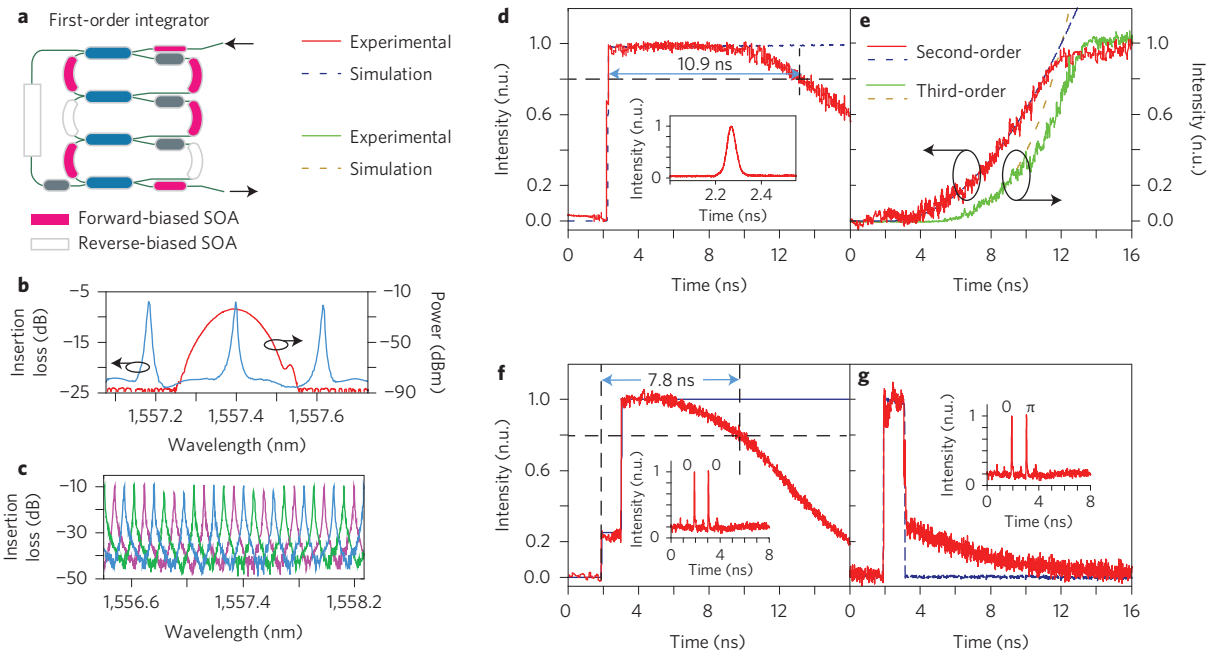

Figure 2 | Experimental results when the photonic integrated signal processor is configured as a temporal integrator. a, The configuration of the first-order integrator. **b**, The spectral response without injection current to the PM in the working ring resonator. **c**, The spectral response of the integrator when the injection current to the PM in the ring is tuned at three different values. **d**, The first-order integration of the Gaussian pulse with an integration time of 10.9 ns. Inset: The input Gaussian pulse with a temporal width of 54 ps. **e**, The second-order and third-order integration of the Gaussian pulse. **f**, The first-order integration of an in-phase doublet pulse, which is shown in the inset. **g**, The first-order integration of an out-of-phase doublet pulse. n.u., normalized unit.

As can be seen an nth-order temporal differentiator has a magnitude response of $|\omega - \omega_0|^n$ and a phase jump of $n\pi$ at ω_0. An optical filter with a frequency response given by (equation (2)) can be implemented using an MZI[23] (see Supplementary Section 3-V). By controlling the coupling coefficients of the input and output couplers in an MZI, a tunable phase shift from 0 to 2π can be achieved, thus a temporal differentiator with a tunable fractional order can be implemented. The photonic integrated signal processor shown in Fig. 1 can be configured to have an MZI structure as shown in Fig. 3a. One arm of the MZI is formed by shutting off the three ring resonators in the unit cell, by applying a reverse bias to one of the two SOAs in each of the three ring resonators. The other arm is the bypass waveguide. The tuning of the fractional order is achieved by changing the coupling coefficients at both the input and output couplers. The operation wavelength can also be tuned by adjusting the injection current applied to the PM in one of the MZI arms.

Photonic temporal Hilbert transformer

A nth-order Hilbert transformer is an LTI system with a transfer function given by[24]

$$H_n(\omega) = \begin{cases} e^{-jn(\pi/2)} & \omega > 0 \\ e^{jn(\pi/2)} & \omega < 0 \end{cases} \quad (3)$$

As can be seen, an nth-order Hilbert transformer has a magnitude response of 1 and a phase jump of $n\pi$ at ω_0. A fractional Hilbert transformer becomes a conventional Hilbert transformer when $n = 1$. For $n = 0$, we have $H_0(\omega) = 1$, which is an all-pass filter. For $0 < n < 1$, the output is a weighted sum of the input signal and its conventionally Hilbert transformed signal[24]. In addition, a fractional Hilbert transformer with an order of n is equivalent to two cascaded fractional Hilbert transformers with fractional orders of α and β if $\alpha + \beta = n$. A ring resonator can be used to implement a Hilbert transformer if the Q-factor is high (see Supplementary Section 3-IV). For a ring resonator with a high Q-factor, the spectral response is close to all pass, except for a narrow notch that is small enough and would contribute negligible error to the transform[25]. Figure 4a shows the configuration. Although the three ring resonators in the processor can be independently enabled or disabled, they are coupled in series. As a result, only one fractional Hilbert transformer or two cascaded fractional Hilbert transformers can be configured in the unit cell corresponding to a single-ring or two-cascaded-ring structure with all-pass configuration.

Results

The proposed signal processor is fabricated in an InP–InGaAsP material system that is wire-bonded to a carrier for experimental demonstration, as shown in Fig. 1c. The SOAs in each ring are measured to have a peak gain of 9.6 dB per SOA, which can be used to compensate for the insertion loss or to shut off the ring. The coupling coefficients of the TCs are measured at different injection currents to the PMs, which can be controlled from 0 to 100% when one of the PMs in each of the TCs is injected with a current from 0 to 3.5 mA (for injection currents applied to each active component, see Supplementary Section 2). There are twenty-one active components (SOAs and PMs) in a unit cell. When injection currents are applied, they will generate heat, which will shift the resonance wavelengths of the ring resonators and degrade the system stability. In the experiment, a temperature control unit is used to ensure the working temperature of the chip is 22 °C, to maintain stable operation.

Integrator. We first test the operation of the signal processor that is configured as a photonic temporal integrator with an order of $n = 1$. As a first-order integrator, the photonic integrated signal processor is configured to operate as a single ring resonator (R1 is on, R2 and R3 are off), as shown in Fig. 2a, where the output optical signal is converted to an electrical signal at a photodetector and monitored by an oscilloscope. The free spectral range (FSR) is measured by an optical vector analyser (OVA, Luna) to be 0.22 nm, as shown in Fig. 2b. By changing the injection current to the PM in the ring (the PM in R1), the spectral response of the ring is laterally shifted, thus the peak location is also shifted, as shown in Fig. 2c,

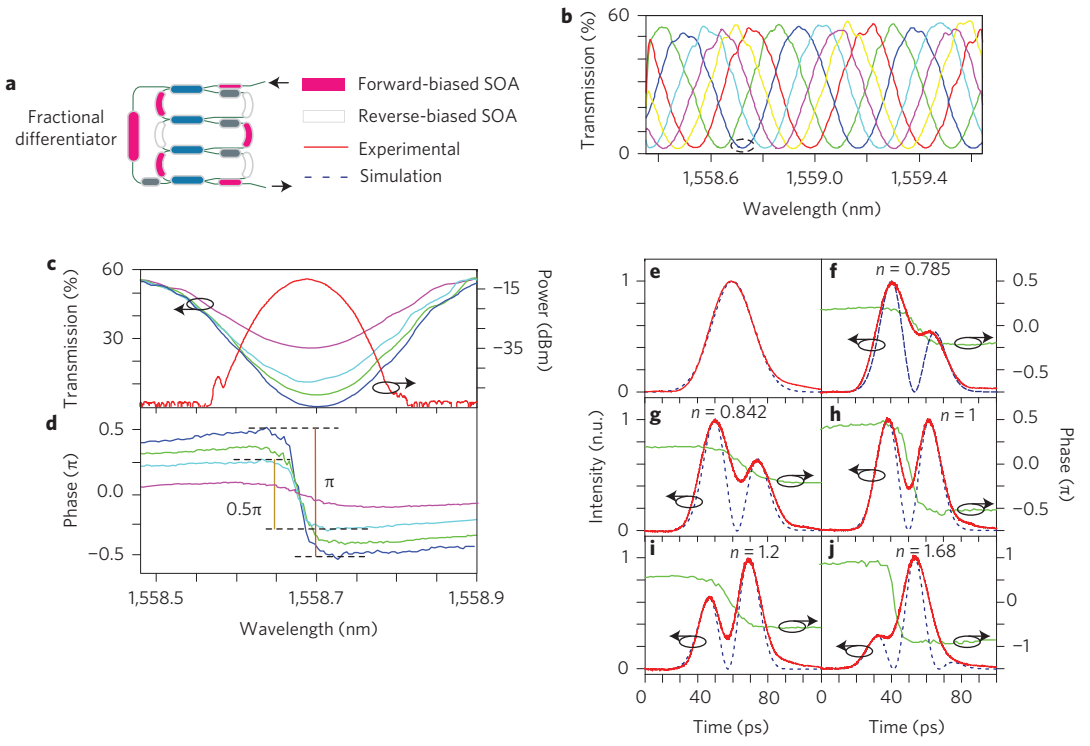

Figure 3 | Experimental results when the photonic integrated signal processor is configured as a fractional differentiator. a, The configuration. **b**, The spectral response with six different injection currents to the PM in the input tunable coupler of the MZI. **c**,**d**, The spectral response (**c**) and phase response (**d**) of the differentiator when the injection current to the PM in the MZI is tuned at four different values. **e**, The input Gaussian pulse with a temporal width of 33 ps. **f**–**j**, The fractional differentiation of the input Gaussian pulse with a fraction order of 0.785 (**f**), 0.842 (**g**), 1 (**h**), 1.2 (**i**) and 1.68 (**j**). n.u., normalized unit.

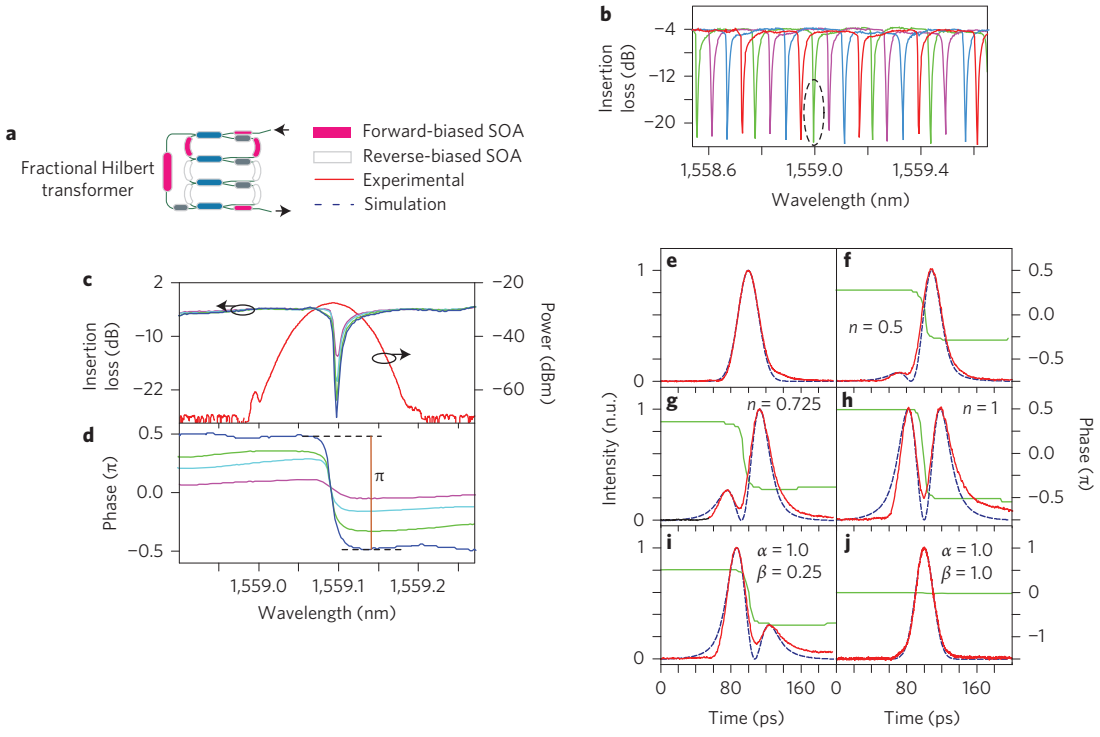

Figure 4 | Experimental results when the photonic integrated signal processor is configured as a Hilbert transformer. a, The configuration. **b**, The spectral response with four different injection currents to the PM in working ring resonator. **c**,**d**, The spectral response (**c**) and phase response (**d**) of the differentiator when the injection current to the PM in the working ring is tuned at four different values. **e**, The input Gaussian pulse with a temporal width of 33 ps. **f**–**h**, The fractional Hilbert transform of the input Gaussian pulse with a fraction order of 0.5 (**f**), 0.725 (**g**) and 1 (**h**). **i**,**j**, The results of the cascaded Hilbert transformers with fraction orders of (1.0, 0.25) and (1.0, 1.0). n.u., normalized unit.

which confirms the tuning of the working wavelength. In the experiment, an optical Gaussian pulse generated by a mode-locked laser (MLL) source and spectrally shaped by an optical bandpass filter (Finisar, WaveShaper 4000S) with a full width at half maximum (FWHM) of 46 ps centred at 1,557.4 nm, as shown as the red curve in Fig. 2b and the inset in Fig. 2d, is then coupled into the temporal integrator via a lensed fibre. Figure 2d shows the first-order temporal integral of the input Gaussian pulse. The integration time is measured to be 10.9 ns, which is more than one order of magnitude longer than the result reported in ref. 15. With a rising time of 48 ps, the proposed photonic integrator offers a time–bandwidth product[15] (TBWP, a principal figure of merit, represents the throughput limit for an optical system determined by the product of the bandwidth and the time–bandwidth of the optical system) of 227, which is much higher than an advanced electronic integrator (TBWP<10)[26], and also more than two-times greater than the previously reported photonic integrator (TBWP~100)[15]. The *Q*-factor is also calculated based on the integration time, which is ~50 million.

Then, the photonic integrated signal processor is configured as a second-order (where R1 and R2 are on and R3 is off), and a third-order (where R1, R2 and R3 are all on) temporal integrator with two and three coupled ring resonators on the chip. The integration of the input Gaussian pulse at the outputs of the second- and third-order temporal integrator is then obtained (Fig. 2e). A higher order integrator, such as a second- and third-order integrator, can be used, for example, to solve higher-order ordinary differential equations[15,16]. A second-order integrator can also be used for arbitrary waveform generation[11]. The first-order integral of an in-phase and out-of-phase doublet pulse is also computed by the proposed first-order temporal integrator. An in-phase/out-of-phase doublet consists of two temporally separated in-phase/out-of-phase Gaussian waveforms with identical amplitude profile. As shown in Fig. 2f,g, the temporal integrator sums up the area under the two field amplitude waveforms for the case of in-phase doublet pulse. As the phase relationship between the two pulses of the in-phase doublet is not maintained during repeated round-trips in the ring resonator due to the dynamic intensity-dependent refractive index variations, the magnitude of the integration output is not well maintained, which leads to a reduced integration time of 7.8 ns. For the case of out-of-phase doublet pulse, the time integral of the second waveform in the doublet pulse cancels that of the first waveform, leading to a square-like profile with the duration determined by the time delay between the two waveforms of the doublet pulse. As shown in Fig. 2g, the two out-of-phase pulses do not subtract completely, this is because the two pulses are not perfectly identical in amplitude and phase due to a slight asymmetry of the MZI used to generate the two pulses (the two pulses are generated by splitting a single pulse to two pulses and recombining the time-delayed pulses at the output of the MZI). These results suggest important applications of a photonic integrator as a memory unit, such as 'write' and 'erase' operations[15]. Simulations are also performed to calculate the temporal integral of the input pulse and the results are plotted with dashed line as shown in Fig. 2d–g. As can be seen, the experimental results agree well with the simulation results. The active components such as the SOAs and PMs in the processor offer a precise control of the resonance peak and the *Q*-factor of each ring resonator, which is indispensable for achieving higher-order integration[8]. This is the first time that a higher order (up to 3) photonic temporal integrator is implemented on an integrated chip.

Differentiator. We test the operation of the signal processor configured to have an MZI structure to operate as a fractional-order temporal differentiator (where R1, R2 and R3 are all off, forming one arm of the MZI, the bypass waveguide forms another arm of the MZI), as shown in Fig. 3a. Again, a photodetector is connected at the output of the chip to convert the optical signal to an electrical signal. The spectral response of the MZI is shown in Fig. 3b. It has an FSR of 0.44 nm. By changing the injection current to the PM in one of the two arms, the spectral response is then laterally shifted, as shown in Fig. 3b. By changing the injection current to the PMs in the tunable couplers at the input or output of the MZI, the coupling coefficient can be tuned to achieve tunable phase shift at the transmission notch. Figure 3c,d shows the measured transmission notch with a phase jump from 0 to π by an optical vector network analyser (OVA, Luna). A Gaussian pulse with a temporal width of 33 ps centred at 1,558.7 nm, shown in Fig. 3c,e, is coupled into the chip. Five differentiated pulses corresponding to five differentiation orders of 0.785, 0.842, 1, 1.2, and 1.68 are obtained, which are shown in Fig. 3f–j, respectively. The phase information of the differentiated pulses is also shown. Again, simulations are also performed to calculate the temporal differentiation of the input Gaussian pulse with five differentiation orders of 0.785, 0.842, 1, 1.2, and 1.68. The results are also shown in Fig. 3f–j. As can be seen, the experimental results agree well with the simulation results. The slight mismatch in the dip between the simulation and experimental output waveforms is due to the limited bandwidth of the photodetector. The proposed differentiator can provide an analog processing bandwidth of 55 GHz, as can be seen from Fig. 4c, which is significant larger than an electronic microwave differentiator[27]. With such a large bandwidth, the photonic differentiator can provide fast signal processing and signal coding[23]. In addition, the differentiation order is also tunable, which provides better flexibility in signal processing, such as tunable image enhancement[28] (see Supplementary Section 4-I).

Hilbert transformer. The photonic integrated signal processor can also be configured to have a single ring or two cascaded ring structure to operate as a fractional Hilbert transformer or two cascaded fractional Hilbert transformers. Figure 4a shows the configuration as a single-ring fractional Hilbert transformer (R1 is on, R2 and R2 are off). The spectral response of the single-ring fractional Hilbert transformer is measured and shown in Fig. 4b with an FSR of 0.22 nm. By changing the injection current to the PM in the ring, the notch location is tuned and the FSR is slightly changed as shown in Fig. 4b. The phase response which determines the fractional order of the Hilbert transform can also be tuned by changing the coupling coefficient between the ring and the bypass waveguide, as shown in Fig. 4c,d, which is achieved by changing the injection current to the PMs in the TCs. To validate the operation of the processor as a fractional Hilbert transformer, an optical Gaussian pulse with a central wavelength at 1,559.1 nm and a temporal width of 33 ps, shown in Fig. 4e, is coupled into the chip. The fractional order of the Hilbert transformer is continuously tunable from 0 to 1 by changing the coupling coefficient through controlling the injection currents to the PMs in the TC. Figure 4f–h shows the fractionally Hilbert transformed pulses with a tunable fractional order from 0.5 to 1. The fractional order Hilbert transformer can be used to construct a secure communication system[24], in which the fractional order n is used as a secret key for demodulation. If the order n is unknown in the demodulation, the signal cannot be recovered. The proposed fractional order Hilbert transformer can also provide fast tunability of the fractional order, which can find applications in secure communication systems.

The signal processor can also be configured as two cascaded Hilbert transformers (R1 and R3 are on, and R2 is off). Figure 4h,i shows the output pulses with the fractional orders of (1.0, 0.25) and (1.0, 1.0) which are equivalent to a single Hilbert transformer with a fractional order of 1.25 and 2. Again, the tuning is achieved by changing the coupling coefficients through controlling the injection currents to the PMs in the tunable couplers. Comparing to the most

recently reported tunable fractional Hilbert transformer in a chip-scale device[10], the proposed Hilbert transformer offers a much easier control of the tunable fractional order through tuning the injection current instead of changing the polarization states of the input signal.

Discussion and summary

The proposed photonic signal processor can be reconfigured as a photonic temporal integrator, differentiator, and Hilbert transformer, which are basic building blocks for general-purpose signal processing (application examples are given in Supplementary Section 4, and performance evaluation is given in Supplementary Section 5). The proposed photonic signal processor can be used to provide high-speed processing to break the speed and bandwidth bottleneck of an electronic processor. For example, a photonic temporal integrator is one of the most important components in a delta-sigma converter for optical analog-to-digital conversion[14]. A photonic temporal differentiator can be used in demultiplexing an OTDM signal[21] and performing real-time amplitude and phase measurement of an optical signal. A Hilbert transformer can be used to generate a wideband SSB modulated signal (see Supplementary Section 4-II), which is useful in a radio-over-fibre (RoF) link to avoid dispersion-induced power penalty[22]. If the designed photonic signal processor is employed in an optical network, the above-mentioned functionalities can be achieved with a single integrated photonic chip. More importantly, with the development of all-optical networks, photonic signal processors can be incorporated into an optical network to perform fast signal processing without digital sampling, and OE and EO conversions. Thus, the proposed photonic signal processor can provide a potential cost-effective solution for signal processing in future all-optical networks.

In summary, we have designed, fabricated and demonstrated a fully reconfigurable photonic integrated signal processor based on a photonic integrated circuit. The operation of the signal processor reconfigured as a temporal integrator, a temporal differentiator and a Hilbert transformer with a tunable order and a tunable operation wavelength was demonstrated experimentally. In particular, a temporal integrator over a bandwidth of 0.22 nm with an integration time of 10.9 ns was achieved, which is the longest integration time ever reported. Although some photonic signal processing functions, such as arbitrary waveform generation and optical dispersion compensation, are not implemented with the current design, this work represents an important step towards the realization of a fully programmable high speed and wideband general-purpose photonic signal processor that can overcome the inherent speed limitation of electronic signal processors.

Methods

Methods and any associated references are available in the online version of the paper.

Received 7 April 2015; accepted 28 December 2015;
published online 15 February 2016

References

1. Kahn, M. *et al.* Ultrabroad-bandwidth arbitrary radiofrequency waveform generation with a silicon photonic chip-based spectral shaper. *Nature Photon.* **4,** 117–122 (2010).
2. Yu, R. *et al.* A scalable silicon photonic chip-scale optical switch for high performance computing systems. *Opt. Express* **21,** 32655–32667 (2013).
3. Willner, A. E., Khaleghi, S., Chitgarha, M. R. & Yilmaz, O. F. All-optical signal processing. *J. Lightw. Technol.* **32,** 660–680 (2014).
4. Koos, C. *et al.* All-optical high-speed signal processing with silicon-organic hybrid slot waveguides. *Nature Photon.* **3,** 216–219 (2009).
5. Weiner, A. M. Ultrafast optical pulse shaping: a tutorial review. *Opt. Commun.* **284,** 3669–3692 (2011).
6. Almeida, V. R., Barrios, C. A., Panepucci, R. & Lipson, M. All-optical control of light on a silicon chip. *Nature* **431,** 1081–1084 (2004).
7. Doerr, C. R. & Okamoto, K. Advances in silica planar lightwave circuits. *J. Lightw. Technol.* **24,** 4763–4789 (2006).
8. Slavík, R. *et al.* Photonic temporal integrator for all-optical computing. *Opt. Express* **16,** 18202–18214 (2008).
9. Ngo, N. Q., Yu, S. F., Tjin, S. C. & Kam, C. H. A new theoretical basis of higher-derivative optical differentiators. *Opt. Commun.* **230,** 115–129 (2004).
10. Shahoei, H., Dumais, P. & Yao, J. P. Continuously tunable photonic fractional Hilbert transformer using a high-contrast germanium-doped silica-on-silicon microring resonator. *Opt. Lett.* **39,** 2778–2781 (2014).
11. Ashrafi, R. *et al.* Time-delay to intensity mapping based on a second-order optical integrator: application to optical arbitrary waveform generation. *Opt. Express* **23,** 16209–16223 (2015).
12. Ngo, N. Q. & Binh, L. N. Optical realization of Newton-Cotes-based integrators for dark soliton generation. *J. Lightw. Technol.* **24,** 563–572 (2006).
13. Hill, M. T. *et al.* A fast low power optical memory based on coupled micro-ring lasers. *Nature* **432,** 206–209 (2004).
14. Reeves, E., Costanzo-Caso, P. & Siahmakoun, A. Theoretical study and demonstration of photonic asynchronous first-order delta-sigma modulator for converting analog input to NRZ binary output. *Microw. Opt. Technol. Lett.* **57,** 574–578 (2015).
15. Ferrera, M. *et al.* On-chip CMOS-compatible all-optical integrator. *Nature Commun.* **1,** 1–5 (2010).
16. Ferrera, M. *et al.* All-optical first and second-order integration on a chip. *Opt. Express* **19,** 23153–23161 (2011).
17. Liu, F. *et al.* Compact optical temporal differentiator based on silicon microring resonator. *Opt. Express* **16,** 15880–15886 (2008).
18. Hillerkuss, D. *et al.* Simple all-optical FFT scheme enabling Tbit/s real-time signal processing. *Opt. Express* **18,** 9324–9340 (2010).
19. Hillerkuss, D. *et al.* 26 Tbit s^{-1} line-rate super-channel transmission utilizing all-optical fast Fourier transform processing. *Nature Photon.* **5,** 364–371 (2011).
20. Li, F., Park, Y. & Azaña, J. Complete temporal pulse characterization based on phase reconstruction using optical ultrafast differentiation (PROUD). *Opt. Express* **32,** 3364–3366 (2007).
21. Slavík, R. *et al.* Demultiplexing of 320 Gbit/s OTDM data using ultrashort flat-top pulses. *IEEE Photon. Technol. Lett.* **19,** 1855–1857 (2007).
22. Sima, C. *et al.* Phase controlled integrated interferometric single-sideband filter based on planar Bragg gratings implementing photonic Hilbert transform. *Opt. Express* **38,** 727–729 (2013).
23. Park, Y., Azaña, J. & Slavík, R. Ultrafast all-optical first- and higher-order differentiators based on interferometers. *Opt. Lett.* **32,** 710–712 (2007).
24. Tseng, C. C. & Pei, S. C. Design and application of discrete-time fractional Hilbert transformer. *IEEE Trans. Circ. Syst. II.* **47,** 1529–1533 (2000).
25. Liu, W. *et al.* in *Proceedings of the Optical Fiber Communications Conference (OFC)* paper Tu2A.6 (Optical Society of America, 2014).
26. Tsai, L.-C. & Fang, H.-S. Design and implementation of second-order microwave integrators. *Microw. And Opt. Tech. Lett.* **53,** 1983–1986 (2011).
27. Hsue, C.-W., Tsai, L.-C. & Chen, K.-L. Implementation of first-order and second-order microwave differentiator. *IEEE Trans. Microw. Theory Tech.* **52,** 1443–1447 (2004).
28. Mathieu, B., Melchior, P., Oustaloup, A. & Ceyral, C. Fractional differentiation for edge detection. *Signal Process.* **83,** 2421–2432 (2003).

Acknowledgements

This work was sponsored by the Natural Sciences and Engineering Research Council of Canada (NSERC). The authors also acknowledge support from the Nanofabrication Center at UCSB.

Author contributions

W.L. analysed the data. W.L., M.L., R.S.G. and J.Y. conceived and designed the experiments. W.L., R.S.G., E.J.N., J.S.P., M.L. and L.C. contributed materials and analysis tools. W.L. performed the experiments. W.L., M.L. and J.Y. wrote the paper.

Additional information

Supplementary information is available in the online version of the paper. Reprints and permissions information is available online at www.nature.com/reprints. Correspondence and requests for materials should be addressed to J.Y.

Competing financial interests

The authors declare no competing financial interests.

Methods

Device fabrication. The designed chip with a single unit cell has a size of 1.5 × 2 mm. In the unit cell, the length of each ring resonator is 3 mm. Two 400-μm SOAs with a confinement tuning layer offset quantum well (CTL-OQW) structure are fabricated in each ring to provide a peak gain of 9.6 dB per SOA to compensate for the insertion loss or to shut off the ring. With the ring length of 3 mm subtracting the length of the two SOAs (400 μm each) in each ring resonator and 7.4 $dBcm^{-1}$ of passive waveguide loss, the total waveguide propagation loss is 1.6 dB for each ring resonator. In addition, each MMI coupler in the ring resonator has 0.5 dB insertion loss. Thus the total round-trip loss is ~3.6 dB, which can be compensated by the SOAs. In the bypass waveguide, there is an SOA with a length of 600 μm to compensate for the insertion loss or to shut off the bypass waveguide. Two additional active SOAs are incorporated into the processor at the input and output waveguides to compensate for the fibre coupling losses, as shown in Fig. 1. In addition, the facets of the bypass waveguides are angled at 7° to minimize the reflections. The peak power of the input optical signal should be below ~13 dBm to avoid damaging the input/output facets. The phase modulation in the ring and the tuning of the coupler are accomplished by forward bias currents via current injection and free carrier absorption through the carrier plasma effect in the PMs. The PMs in the chip are fabricated with a length of 300 μm.

The chip was fabricated on a quarter of a wafer that was grown at UCSB. At the beginning, the areas in the chip for the SOAs, passive (low loss waveguide propagation), and phase modulator, are defined by using semiconductor wet-etching techniques. After regrowth, the deeply-etched waveguides are defined. The waveguide etch is performed using a 200 °C ICP-RIE dry etch. To make contact to SOAs and PMs, vias need to be constructed and metallization applied to the device. First, the newly-etched sample is coated in 300 nm of silicon nitride using PECVD. This provides the electrical insulation required such that metal traces and pads can be placed on the surface of the photonic integrated chip (PIC). Then, a partial exposure is performed on sections of waveguide where vias are desired.

To ease testing, the chips need to be cleaved apart and made secure on a carrier for wire bonding. The carrier provides structural integrity and large pads for probing with probe cards. The individual devices are mounted with solder onto an aluminum nitride carrier and then wire-bonded to the carrier pads.

Pulse generation and measurement. We used a mode-locked laser source with a repetition rate of 48.6 MHz and a central wavelength at 1,558.7 nm to generate an optical pulse, and the pulse width is controlled by a programmable optical filter (Finisar, WaveShaper 4000S) connected at the output of the mode-locked laser source. The in-phase and out-of-phase doublet pulses are generated using an unbalanced MZI by launching an optical Gaussian pulse into the MZI with a length difference between the two arms of 25 cm. As a result, two closely separated pulses with a temporal separation of 1.14 ns are generated. Depending on the phase shift applied to one pulse by a phase modulator in one arm of the MZI, an in-phase (no phase shift) or out-of-phase (π phase shift) doublet pulse is generated.